COMMISSIONING OF A HIGH-GRADIENT X-BAND RF GUN POWERED BY SHORT RF PULSES FROM A WAKEFIELD ACCELERATOR*

W. H. Tan†, X. Lu[1], P. Piot[1], Northern Illinois University, DeKalb, IL, USA

C. Jing[1], S. Antipov, S. Kuzikov, E. Knight, Euclid Techlabs LLC, Bollingbrook, IL, USA

D. S. Doran, W. Liu, J. G. Power, C. Whiteford, E. E. Wisniewski,

G. Ha, J. Shao, Argonne National Laboratory, Lemont, IL, USA

[1] also at Argonne National Laboratory, Lemont, IL, USA

Abstract

A high-gradient *X*-band (11.7-GHz) photoinjector developed by Euclid Techlabs, was recently commissioned at the Argonne Wakefield Accelerator (AWA). The system comprises a 1+1/2-cell RF gun powered by short RF pulses generated as a train of high-charge bunches from the AWA accelerator passes through a slow-wave power extraction and transfer structure. The RF photoinjector was reliably operating with electric fields in excess of 300 MV/m on the photocathode surface free of breakdown and with an insignificant dark-current level. We report on the RF-gun setup, commissioning, and the associated beam generation via photoemission.

INTRODUCTION

Bright-electron sources have a wide range of applications in accelerator-based light sources and electron probes, such as free-electron lasers (FELs) and ultrafast electron diffraction. The report of Basic Energy Sciences Workshop on the Future of Electron Sources in 2016 identified *High-gradient R&D for next generation electron sources* as one of four Priority Research Directions in the future electron sources [1]. It had anticipated in 5 years the realization of a factor of two higher electric field than the well-established 100 MV/m S-band RF photoinjector thus enabling the next generation electron source with ~ 100-pC and ~ 30-nm emittance for the most demanding applications. A critical aspect to the generation of bright electron beams is the use of high gradient radiofrequency (RF) gun on suppressing space charge effects during the photoemission process. Accordingly, the beam peak brightness $\mathcal{B} = q/\Gamma$, where q is the bunch charge and Γ its six-dimensional phase-space volume, scales with the applied electric field E_0 on beams during emission at the emitter surface as $\mathcal{B} \propto E_0{}^\alpha$ where the exponent $\alpha \geq 1$ depends on the bunch's initial transverse-to-longitudinal aspect ratio [2, 3]. One path toward producing high-gradient electric fields for bright electron beam generation consists of operating a RF gun at higher frequencies. Such an approach is limited by the RF breakdowns where field-emitted electrons due to surface imperfection leads to local RF-induced heating and damage the cavity wall. The RF breakdown can be described by a phenomenological model where the

breakdown rate (BDR) is described by BDR $\sim E_0{}^{30}\tau_p{}^5$, where E_0 is the applied electric on the surface and τ_p is the length of the RF pulse [4–6]. From the equation, it is implies that the breakdown rate of a high gradient RF gun can be reduced by shortening the RF pulse duration. Although this approach has been proposed more than a decade ago its implementation to realize short sub-100-ns RF pulse has remained elusive so far.

A high gradient X-band RF (XRF) gun was designed by Euclid Techlabs LLC and commissioned at the Argonne Wakefield Accelerator (AWA) facility [7–10]. This gun operates at 11.7 GHz driven by short RF pulses generated via the deceleration of high charge electron beams passing through a power extraction and transfer structure (PETS) available at the AWA facility. In this paper, we report the setup, commissioning of this XRF gun along with the generation of ~ 100 pC relativistic (~ 3 MeV) electron bunches.
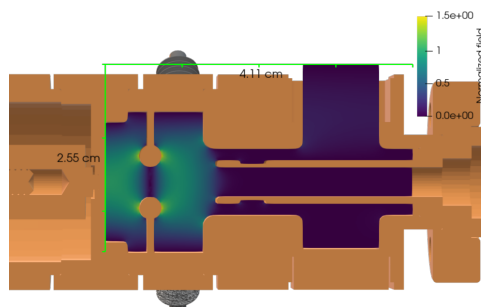
Figure 1: Cross section of the XRF gun superimposed with the applied electric field.

PHOTOINJECTOR SETUP AND DESIGN

The cut-away of the XRF gun appears in Fig. 1 with a superimposed electric-field amplitude map. The gun consists of $1 + \frac{1}{2}$-cell RF cavity oprating on the $TM_{010,\pi}$ mode. The iris includes four magnetic coupling slots to increase both the RF coupling between cells and the frequency separation from the neighboring resonant $TM_{010,0}$ mode. The cavity is strongly over-coupled resonator resulting in loaded Q of factor ($Q_\ell \simeq 180$), thus allowing for the rapid build-up of field inside of the cavity. The gun is made of oxygen-free copper using conventional fabrication techniques. A broadband coaxial RF-input coupler is used to ensure the field remains axi-symmetric. The X-band photoinjector beamlines is diagrammed in Fig. 2. The photoinjector consists
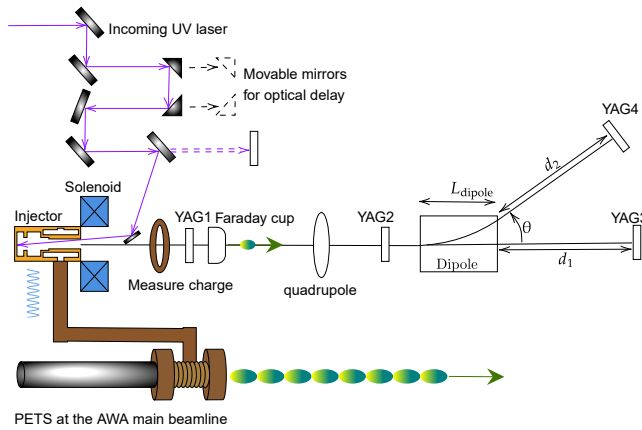
Figure 2: Diagram of the XRF photoinjector beamline. The incoming UV laser is directed into the XRF gun for photoemission the beam distribution can be measured on YAG screens.

of the XRF gun, a magnetic solenoid lens, and other beam diagnostics tools. Several YAG screens were installed to provide diagnostics at various locations along the beamline. An integrated current transformer (ICT) and a Faraday cup were installed just downstream of the XRF gun to measure the bunch charge. A quadrupole magnet were provide transverse focusing. Finally, a magnetic dipole to serve as a spectrometer for energy measurement.

The XRF gun operates at 11.7 GHz selected to match the PETS available in AWA main beamline. The generates short RF pulses when 8 highly charged ($\sim$ 50 nC) electron bunches passing through the PETS. The RF-pulse duration is $\sim$10 ns (full width) with a 3-ns flat top and the input power was measured at $\sim$250 MW in Ref. [11].

The electron bunch were generated using the AWA photocathode laser. The UV laser pulse was split with most of the energy sent to the AWA drive-beam gun and a fraction < 200 µJ directed toward the XRF gun. The UV path to the XRF-gun photocathode include a movable delay stage used to time the laser pulse to reach the photocathode when the field is maximum.

BEAM GENERATION AND PHASE SCAN

During the experiment, short RF pulses were fed from the AWA main beamline to operate the XRF gun. Movable mirrors were adjusted to perform phase scans. The electron beam transverse profile was measured at YAG1; see Fig. 3.

Subsequently, a throughout phase scan was performed to investigate the relation between phase and measured charge. Figure 4 present such a phase scan over two emission periods (corresponding to two X-band RF buckets). For these scans the charge was directly measured from the ICT. The zero-crossing phase was used as a reference (corresponding to $\varphi = 0°$ in Fig. 4). The uncertainty on the phase resolved using the optical delay step was estimated to be $\Delta\varphi_0 \simeq 7°$ (at 11.4 GHz).
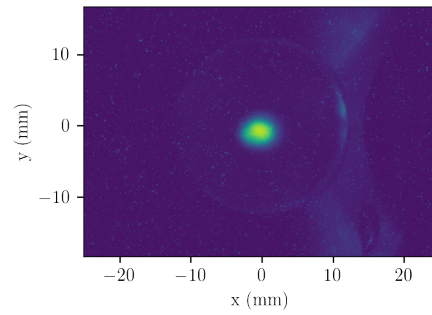
Figure 3: Transverse beam distribution on the YAG1 screen; see Fig. 2. The bunch charge is approximately 100 pC.
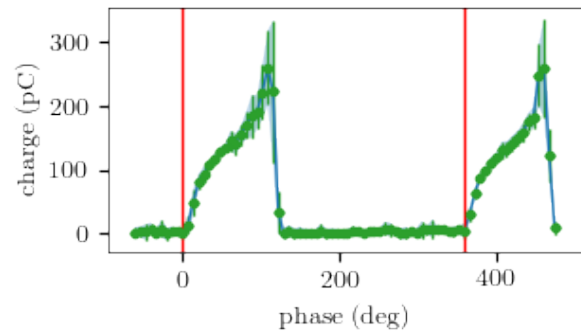
Figure 4: Phase scan was performed by adjusting optical path with movable mirrors. Charge values of electron beams were measured using ICT. Reference points of the 0° and 360° phases were set at the location where photoemission just started to occur on both emission periods, as shown from red lines.

The evolution of the emitted charge over the course of emission periods shows the characteristic of Schottky's enhanced photemission, resulting from the presence of high electric field gradients that lowers the potential barrier at the cathode surface [12]. We observed Schottky's enchaned photoemission, as shown in spikes from Fig. 4 near 100° and 450°.

ENERGY MEASUREMENT AND FIELD INFERENCE

The energy measurement is using a spectrometer (labeled as "dipole" located between YAG2 and YAG3 in Fig. 2). The energy-measurement procedure consists in centering the beam in YAG2 and YAG3 with the dipole magnet turned off and degaussed. The dipole magnet current is then slowly ramped until the beam position is horizontally centered at YAG4. Such a condition ensures the beam center follows the reference trajectory in the dipole, i.e. the design bending radius, so that the applied magnetic field B and reference-particle (beam center) momentum p_0 verifies $B\rho = p_0 c$, where c is the speed of light and ρ is the radius of curvature of the trajectory in the dipole. The momentum can be extracted from the applied B field via $p_0 c = \frac{BL_{\text{eff}}}{\sin\vartheta}$, where the effective

length was computed from the 2-D field map to be $L_{eff} = 0.308$ m and the nominal bending angle is $\vartheta = 20°$ by design so that the design bending radius is $\rho = \frac{L_{eff}}{\sin(\vartheta)} = 0.901$ m. The uncertainty on the B field is essentially instrumental, while the uncertainty on the angle comes from misalignment of the incoming beam (when centering the beam on YAG2 and 3) we estimate the error on the angle to be approximately $\partial\vartheta \simeq \frac{1 \times 10^{-2}}{0.8} \simeq 1.1 \times 10^{-2}$ rad. From the latter equation we expect the relative error on the momentum measurement to be approximately

$$\frac{\partial p_0}{p_0} = \left[\frac{(\partial B)^2}{B^2} + \frac{(\partial\vartheta)^2}{\tan^2\vartheta} \right]^{1/2}, \quad (1)$$

where the uncertainty coming from the angle is approximately $\frac{|\partial\vartheta|}{\tan\vartheta} \simeq 1.7 \times 10^{-2}$. The magnetic field is obtained from the current setpoint as $B = (182.6 \pm 0.1)I$ so that we expect $\frac{\partial B}{B} \simeq 5 \times 10^{-4}$ implying that the uncertainty is dominated by the alignment tolerance ($\partial\vartheta$) on the beam trajectory in the spectrometer line. In the following we report kinetic energy instead of momentum as $K = \sqrt{p_0^2 c^2 + (mc^2)^2} - mc^2$, where mc^2 is the electron's rest mass and correspondingly perform the error propagation. An example beam position and retrieved kinetic energy measured at YAG4 appear in Fig. 5. The measurement indicates that kinetic energy close
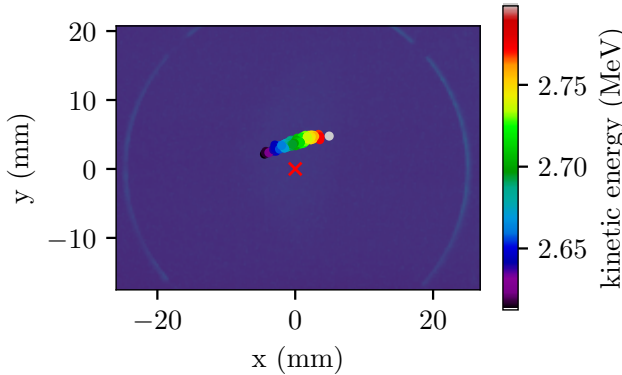
Figure 5: A plot of beam centroids overlaying on YAG4 screen, with colorbar representing the inferred kinetic energy.

to 3 MeV are reached.

The energy measured downstream of the gun is a non-linear function of the field applied on the cathode surface E_0 and the laser-launch phase φ [13, 14]. As a first step we implemented the longitudinal equation of motion in a simple one-dimensional model of the beam dynamics by numerical solving the coupled ODEs

$$\begin{cases} \frac{dp_z}{dt} = eE_0 \mathcal{E}_z(z) \cos(\omega t + \varphi), \\ \frac{dz}{dt} = \frac{p_z}{m\gamma} \end{cases} \quad (2)$$

for a single electron. Here we neglect the transverse dynamics and assume $p_x = p_y = 0$, and the trajectory of the electron remains on axis and not subjected to any transverse force.

In the latter equation $\mathcal{E}_z(z)$ represents the peak-normalized axial field profile on axis (e.g. obtained from an electromagnetic eigensolver) and γ is the Lorentz factor. By solving Eq. 2. We ultimately used ASTRA [15] to numerically compute the function $K(E_0, \varphi_0)$ over a 28×86 two-dimensional grid for $E_0 \in [315, 450]$ MV/m and $\varphi_0 \in [45°, 130°]$. A spline-interpolated function $K(E_0, \varphi_0)$ was then used to calculate the value of E_0 given the measured kinetic energy and operating phase φ_0. The contour plot of $K(E_0, \varphi_0)$ and an example of inferred field value appear in Fig. 6. The area enclosed by two kinetic-energy isoclines and two vertical lines of operating phase, obtained from measurement uncertainties, provide the error region of the calculated field with its upper and lower error bounds. The result of such an analysis confirms that the maximum peak field attained during our experiment was $E_0 = 387.76^{+44.63}_{-35.88}$ MV/m.
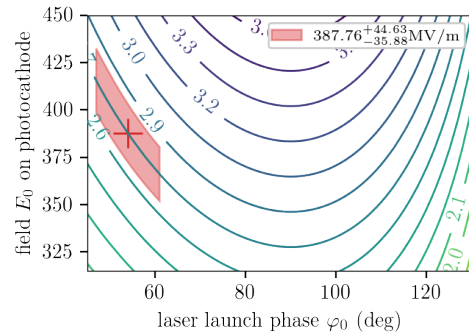
Figure 6: Plot of kinetic-energy isocline as a function of E-field on photocathode and laser launch phase. Red cross is the measured beam energy and red shaded area is the error region. The inferred field gradient in this example is $387.76^{+44.63}_{-35.88}$ MV/m.

CONCLUSION

In summary, the XRF gun was successfully commissioned at the AWA. A photoinjector beamline was built and used to investigate electron-beam generation and performed beam-based measurement of the photocathode surface field. The experiment demonstrated the reliable generation of field close to 400 MV/m on the photocathode over a two-week running period. Furthermore the experiment did not suffer from any breakdown (the upper limit for the BDR is estimated to 1×10^{-5}. Additionally, no dark current could be measured. The results obtained so far confirmed that use of short RF pulse to power an electron source offer a viable path toward producing the bright electron beams.

REFERENCES

[1] X. Wang, P. Musumeci, E. Lessner, and J. Goldstein, "Report of the basic energy sciences workshop on the future of electron sources, September 8-9, 2016," 2016, https://www.osti.gov/biblio/1616511, doi:10.2172/1616511

[2] I. V. Bazarov, B. M. Dunham, and C. K. Sinclair, "Maximum achievable beam brightness from photoinjectors," *Phys. Rev. Lett.*, vol. 102, p. 104 801, 10 2009, doi:10.1103/PhysRevLett.102.104801

[3] D. Filippetto, P. Musumeci, M. Zolotorev, and G. Stupakov, "Maximum current density and beam brightness achievable by laser-driven electron sources," *Phys. Rev. ST Accel. Beams*, vol. 17, p. 024 201, 2 2014, doi:10.1103/PhysRevSTAB.17.024201

[4] A. Grudiev, S. Calatroni, and W. Wuensch, "New local field quantity describing the high gradient limit of accelerating structures," *Phys. Rev. ST Accel. Beams*, vol. 12, p. 102 001, 10 2009, doi:10.1103/PhysRevSTAB.12.102001

[5] S. Döbert *et al.*, "High Power Test of an X-Band Slotted-iris Accelerator Structure at NLCTA," *Conf. Proc. C*, vol. 070625, p. 2191, 2007, doi:10.1109/PAC.2007.4441193

[6] F. Wang, "Breakdown characteristics study on an 18 cell X-band structure," *AIP Conference Proceedings*, vol. 1086, no. 1, pp. 373–379, 2009, doi:10.1063/1.3080934

[7] S. Kuzikov, S. Antipov, P. Avrakhov, G. Ha, A. Liu, and J. Power, "Ultra-High Gradient Short RF Pulse Gun," in *10th International Particle Accelerator Conference*, Melbourne, Australia, May 2019, pp. 2987-2989. doi:10.18429/JACoW-IPAC2019-WEPRB072

[8] W. H. Tan *et al.*, "Demonstration of sub-GV/m Accelerating Field in a Photoemission Electron Gun Powered by Nanosecond *X*-Band Radiofrequency Pulses," 2022, doi:10.48550/ARXIV.2203.11598

[9] M. Peng *et al.*, "Generation of High Power Short Rf Pulses using an X-Band Metallic Power Extractor Driven by High Charge Multi-Bunch Train," in *Proc. 10th Int. Particle Accelerator Conf.*, Melbourne,Australia, May 2019, pp. 2987-2989. doi:10.18429/JACoW-IPAC2019-MOPRB069

[10] J. H. Shao *et al.*, "Demonstration of Gradient Above 300 MV/m in Short Pulse Regime Using an X-Band Single-Cell Structure," Bangkok, Thailand, Jun. 2022, 13, presented at IPAC'22, Bangkok, Thailand, Jun. 2022, paper FROXSP2, this conference.

[11] J. Shao *et al.*, "High-Power Test of a Highly Over-Coupled X-Band RF Gun Driven by Short RF Pulses," in *Proc. IPAC'21*, Campinas, SP, Brazil, May 2021, pp. 4432– 4434, doi:10.18429/JACoW-IPAC2021-THPAB331

[12] W. Schottky, "Über kalte und warme elektronenentladungen," *Zeitschrift für Physik*, vol. 14, no. 1, pp. 63–106, 1923, doi:10.1007/BF01340034

[13] K.-J. Kim, "RF and space-charge effects in laser-driven RF electron guns," *Nuclear Instruments and Methods in Physics Research Section A: Accelerators, Spectrometers, Detectors and Associated Equipment*, vol. 275, no. 2, pp. 201–218, 1989, doi:https://doi.org/10.1016/0168-9002(89)90688-8

[14] K. Flöttmann, "RF-induced beam dynamics in RF guns and accelerating cavities," *Phys. Rev. ST Accel. Beams*, vol. 18, p. 064 801, 6 2015, doi:10.1103/PhysRevSTAB.18.064801

[15] K. Flöttmann, *Astra a space charge tracking algorithm, version 3.2*, available from DESY, Hamburg, Germany, 2017, https://www.desy.de/~mpyflo/

MC3: Novel Particle Sources and Acceleration Techniques

T02: Electron Sources